sustainable chemistry

MDPI

Article

SBA-15 Modified with Tethered Ionic Liquids Applied in the Esterification of Valeric Acid with Pentanol—Towards Cellulosic Biofuels

Lisa Mullins and James A. Sullivan *

UCD School of Chemistry, University College Dublin, Belfield, Dublin 4, Ireland; lisa.mullins@ucdconnect.ie

* Correspondence: james.sullivan@ucd.ie

Received: 17 July 2020; Accepted: 3 September 2020; Published: 5 September 2020

Abstract: Two catalysts are prepared by tethering ionic liquid cation components (1-(propyl-3-sulfonate)-3-(3-trimethoxysilylpropyl) imidazolium) with either chloride or sulphate anions, to the surface of a mesoporous SiO_2 material through a condensation reaction. These are characterized using elemental analysis, TGA-MS, FTIR (and D-FTIR), TEM, physisorption and NH_3 adsorption (TPD and FTIR), and applied in the valeric acid + pentanol esterification reaction to form the sustainable biodiesel Pentyl Valerate. The material containing the sulfate counter-ion was significantly more active than the chloride analogue.

Keywords: green catalysts; biorefinery; catalytic conversion; cellulose; biofuels

1. Introduction

The combustion of petroleum-derived diesel contributes to the increase in atmospheric CO_2 and depletes finite fossil fuel reserves [1]. Theoretically, the use of biodiesel should solve both problems as the fuel feedstock would be continuously replenished (concomitantly removing CO_2 from the atmosphere as it does so, nominally making the process carbon neutral). While Fatty Acid Methyl Esters (FAME) generated from the transesterification of vegetable oils can be used as replacements for petroleum-derived diesel, and their production and the transesterification reaction received significant research interest on that basis [2–4], their use is not considered sustainable when aspects such as fertilizer use, biomass waste, the food versus fuel debate and the non-sustainability associated with the geographical areas in which high yielding vegetable oils can be grown are compared with areas in which bio-fuels are predominantly used are considered [5].

This has led to research into more sustainable bio-replacements than FAME and the use of cellulose as a feedstock. Cellulose is much more sustainable a feedstock than triglycerides, forms the bulk of several types of biomass, requires low levels of fertilizer to grow, and can be produced on relatively infertile soils [6]. Cellulose can be converted into levulinic acid (at about 50% yield) using the Biofine process [7] meaning that levulinic acid is a platform molecule which can be sustainable in biorefining processes to generate fuels and chemicals.

One possible use of levulinic acid is to convert it to pentanoic acid (also known as valeric acid–VA), subsequently convert a fraction of this to pentanol, and esterify the acid and alcohol to form pentyl valerate (PV) [8,9] (another molecule that has the flow and combustion characteristics of diesel).

Normally esterification reactions are carried out using acidic catalysts [10,11] and this work looks at two acidic catalysts prepared through the tethering of an ionic liquid cation containing a sulfonic acid group (using two different counter-ions) to an SBA-15 surface and analyzing their activity in the esterification reaction.

ILs are attractive solvents and catalysts due to their interesting properties such as low vapor pressure, high catalytic activity, ability to dissolve a wide range of organic and inorganic compounds,

and their ease of recyclability [12,13]. There are also some drawbacks associated with ILs, one of them being their high viscosity resulting in mass transfer issues when used as reaction solvents.

Recent research has shown that the tethering/immobilization of ILs onto the surface of solid supports (and use of a standard solvent) avoids this problem [14,15]. For example, Zhang et al. have tethered an IL onto the surface of SBA-15 and used it for the catalytic synthesis of the bio-diesel product methyl oleate with a conversion of 90% from oleic acid [16]. This has been extended to other supports and IL cations in related reactions [17–19].

This concept of tethering an IL to SBA-15 mesoporous SiO_2 to generate a material to promote the pentanol/pentanoic acid esterification will be described in this contribution and specifically we will concentrate on the role of the IL counter-ion in controlling reactivity.

2. Materials and Methods

2.1. Catalyst Preparation

2.1.1. Synthesis of mesoporous silica (SBA-15)

Pluronic (4 g) was added to HCl (2 M, 120 mL) and distilled H_2O (30 mL). This was stirred at room temperature until dissolved (approx. 3 h). The temperature was raised to 40 °C and TEOS (8.5 g, 0.041 mol) was added, and the solution stirred for 20 h. The reaction mixture was then aged under static conditions at 80 °C for 24 h. The mixture was filtered, washed with distilled H_2O, and dried in the oven. The white powder was calcined at 600 °C for 6 h [20,21].

2.1.2. Synthesis of 1-(propyl-3-sulfonate)-3-(3-trimethoxysilylpropyl) imidazolium hydrogen sulfate/chloride ([SO_3H-PIm-CPMS][HSO_4]), (IL-HSO_4-SBA-15 or IL-Cl-SBA-15), an acidic Ionic Liquid (IL).

This followed the process reported by Zhang et al. [16]. Imidazole (1.36 g, 0.02 mol) (Sigma-Aldrich >99%) and sodium ethoxide (1.36 g, 0.02 mol) (Sigma-Aldrich >95%) were placed in ethanol (30 mL) and stirred at 80 °C for 8 h. N_2 gas was then flowed through the system to create a nitrogen atmosphere and the system sealed. (3-Chloropropyl)trimethoxysilane, CPMS (3.96 g, 0.02 mol) (Sigma-Aldrich >99.9%) was added dropwise and the solution was stirred for 16 h. The byproduct NaCl (white precipitate) was filtered off, 1,3-propane sultone (2.45 g, 0.02 mol) (Sigma-Aldrich >99%) was added and the reaction mixture stirred at 50 °C for 16 h. Depending on which counter-ion was desired either, H_2SO_4 (1.94 g, 0.02 mol) or HCl (0.74 g, 0.02 mol) was added dropwise over 30 min. The solution was then stirred for a further 6 h. The product was filtered and washed with diethyl ether. The filtered product was then subjected to rotary evaporation to remove excess ethanol and diethyl ether. See Figure 1 for a schematic showing the production of the version with the HSO_4^- counterion.

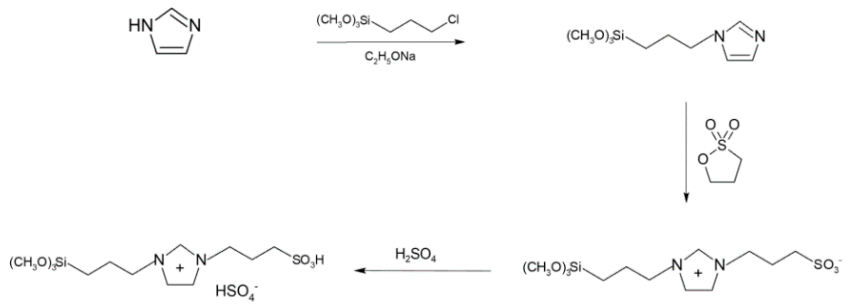

Figure 1. The synthesis of 1-(propyl-3-sulfonate)-3-(3-trimethoxysilylpropyl) imidazolium hydrogen sulfate (IL-HSO_4-SBA-15). The (IL-Cl-SBA-15) catalyst was prepared in a similar manner except HCl rather than H_2SO_4 was used in the final step.

2.1.3. Synthesis of Ionic liquid functionalized SBA-15 (IL-HSO_4-SBA-15 or IL-Cl-SBA-15).

During the SBA-15 functionalization reactions, attempts were made to achieve tethering which resulted in 2% (wt%) sulfonic acid on the surface of both catalysts (assuming 100% incorporation of the condensing silane).

The acidic ionic liquid (IL) (0.35/0.32 g (HSO_4^-/Cl^-), as prepared above was placed in toluene (100 mL) to which SBA-15 (1 g) was added. The solution was refluxed at 130 °C for 24 h. The product was then filtered off and washed with distilled water.

2.2. Catalyst Characterizations

The elemental analysis was carried out using a CHNS-O 4010 Elemental Combustion System, N_2 adsorption and desorption isotherms were measured on a Micromeritics ASAP 2020. Samples were degassed overnight at 120 °C prior to measurement.

TEM images were obtained using a Technai G2 20 Transmission Electron Microscope with a variable operating accelerating voltage up to 200 kV. Samples were prepared for TEM analysis by dispersal and sonication in ethanol. A drop of this suspension was pipetted onto a copper TEM grid. The ethanol was evaporated off before samples were imaged. Image J software was used to calculate pore sizes/particle sizes of materials.

To measure surface OH concentration [22] and confirm tethering TGA/MS experiments were performed on Q500 TGA (TA Instruments) coupled to a HPR20-QIC Atmospheric Gas Analysis System (Hiden Analytical). TGA/MS experiments were carried out as follows; the pan was tared and loaded with 5–20 mg of the sample to be analyzed. The pan was enclosed in the furnace, held isothermally for 30 min at room temperature, and the temperature then ramped to 900 °C, at a rate of 10 °C min^{-1}. Samples were held under a flow of air (90 mL min^{-1}) and nitrogen (10 mL min^{-1}) (balance gas, which flows over the electronics of the instrument). Portions of the exit gas were continuously analyzed by the online mass spectrometer.

FTIR measurements were carried out on a Vertex 70 FTIR spectrometer equipped with a Globar Infrared source for a spectral range in the NIR-MIR, a DRIFTS cell (Praying Mantis), and a liquid nitrogen cooled mercury cadmium telluride (MCT) detector. In certain experiments (probing acidity) NH_3 was pre-adsorbed to the surface of the catalyst prior to the collection of the FTIR spectrum, and in these cases the catalyst was used as the spectral background. The catalyst sample was treated at 100 °C under a flow of inert gas, argon/nitrogen, at 100 mL min^{-1} for 1 h to remove any adsorbed water from the catalyst surface. The sample was cooled to room temperature, a background spectrum recorded, and the sample then heated to 30 °C. The system setup allowed for the flow of argon/nitrogen to be reduced to a flow of 60 mL min^{-1} and the probe gas (NH_3) introduced over the sample at a flow of 40 mL min^{-1} for 15 min. This allowed for a total gas flow of 100 mL min^{-1} to be maintained. After saturation with the probe, the flow of NH_3 was replaced with argon/nitrogen and left at 30 °C for a further 30 min to remove the physisorbed fraction of the probe molecules. The sample was again cooled to room temperature and a difference spectrum recorded.

Acidity measurements—A number of other techniques were used to measure the concentration and strength of surface acid sites on the materials.

The NH_3 temperature programmed desorption −20 mg of catalyst was loaded into a glass tube (held between two plugs of quartz wool) and the tube was placed inside a furnace. The catalyst was held in a flow of inert gas argon/nitrogen (100 mL min^{-1}) for 30 min at 100 °C to remove any physisorbed species from the surface of the catalyst. The sample was then cooled down to 50 °C before dosing with the probe gas NH_3 (1% in He). The system was allowed for the flow of argon/nitrogen to be reduced to a flow of 60 mL min^{-1} and the NH_3 was introduced over the sample at a flow of 40 mL min^{-1}. This allowed for a total gas flow of 100 mL min^{-1} to be maintained at all times. Once the surface of the catalyst was saturated with NH_3 (monitored using online mass spectrometry (Thermo Onix)) it was removed from the flow and replaced with argon/nitrogen. The sample was then cooled to 30 °C and held at this temperature until the NH_3 signal returned to the baseline (removal of the

physisorbed fraction). The sample was then heated from 30 to 750 °C at a rate of 20 °C min^{-1} and the exit gas was continuously monitored by online mass spectrometry. Fragments at m/z = 4 (He), 14 (N), 16 (O), 17 (OH/NH_3), 18 (H_2O), 28 (N_2), 30 (NO), 40 (Ar), 44 (CO_2/N_2O), and 46 (NO_2) were recorded as a function of temperature.

Hammett indicators were also to be used to determine surface acid strength [23]. Typical acid strength experiments were carried out as follows; 0.1 g of dried solid acid catalyst was added to a vial, and a 0.1% solution of indicator in benzene was added (three drops in the case of all indicators). The color of the absorbed indicator was noted, and this allowed determination of whether the catalyst was basic or acidic relative to the different indicators (and thus if it had a Hammett acidity function H_0 lying between the *p*Ka's of two indicators).

Acid capacity measurements determined the acid concentration of the different materials. In a typical acid capacity measurement 0.1 g of acid catalyst was added to 10 mL of deionized water. The resulting suspension was allowed to equilibrate (stirred for 30 min) and thereafter was titrated by dropwise addition of NaOH (0.01 M) using phenolphthalein (0.5 wt% in ethanol and water (1:1)) as an indicator with a color change from cloudy white to cloudy pink indicating the endpoint.

2.3. Catalytic Measurements

The esterification reaction was carried out as follows: Valeric Acid, VA (1.7 mL, 0.016 mol) and pentanol, V-OH (15 mL, 0.14 mol) were added to a 25 mL round bottom flask and stirred. The reaction mixture was heated to 120 °C under reflux and stirring. Once the system reached the desired temperature an aliquot was removed for analysis. The catalyst (100 mg) was then added and sampling of the reaction mixture was carried out periodically over 5 h.

The reaction analysis was carried out using a Shimadzu G-17a with a Cp-Sil 5CB capillary (dimethylpolysiloxane) column and a flame ionization detector (FID). For analysis, the injector temperature was held at 200 °C, while the FID was held at 300 °C. The initial temperature of the column was set to 70 °C and a temperature programmed run was carried out at a rate of 10 °C min^{-1} to 250 °C.

An internal standard (octanol) was used to account for variations in GC responses for both the analysis of standard solutions and reaction mixtures.

Typically, the reaction analysis involved a periodic extraction of an known volume of the reaction mixture and addition of an equal volume of internal standard. This was followed by sonication to ensure the solutions were fully mixed. One μL of this was then injected directly onto the column using a 1 μL syringe.

3. Results and Discussion

3.1. Catalyst Characterization

The elemental analysis confirms the absence of C, S, and N on the parent SBA-15 material, and the presence of these elements on IL-HSO_4-SBA-15, and IL-Cl-SBA-15 at levels close to those theoretically expected (see Table 1). The level of S on the IL-HSO_4-SBA-15 material is almost twice that on the IL-Cl-SBA-15 material (reflecting the S atoms also present in the former material's counter-ions).

Table 1. C, S, and N levels found on the IL-HSO_4-SBA-15 and IL-Cl-SBA-15 catalysts following elemental analysis, and S_{BET}, pore volume, and average pore diameters of tethered of materials following N_2 physisorption (see Figure 2).

Catalyst	%C Measured (Theory)	%S Measured (Theory)	% Measured (Theory)	$S_{BET}/m^2\ g^{-1}$	Pore Volume/mL g^{-1}	Pore Diameter/nm
SBA-15	0.00	0.00	0.00	552	0.5	4.3
IL-HSO_4-SBA-15	4.47 (4.43)	4.60 (4.58)	1.39 (1.50)	383	0.4	5.0
IL-Cl-SBA-15	5.81 (5.40)	2.96 (2.40)	1.34 (1.80)	234	0.4	6.1

Figure 2 shows (a) displaced BET adsorption/desorption isotherms for SBA-15 (red), IL-Cl-SBA-15 (orange), IL-HSO_4-SBA-15 (purple), and (b) the corresponding pore size distribution profiles obtained by applying the BJH method to the desorption branch of the isotherm (the numbers beside the peaks indicate the pore diameter at the maximum point). Table 1 shows the corresponding BET surface areas, pore sizes, and volumes.

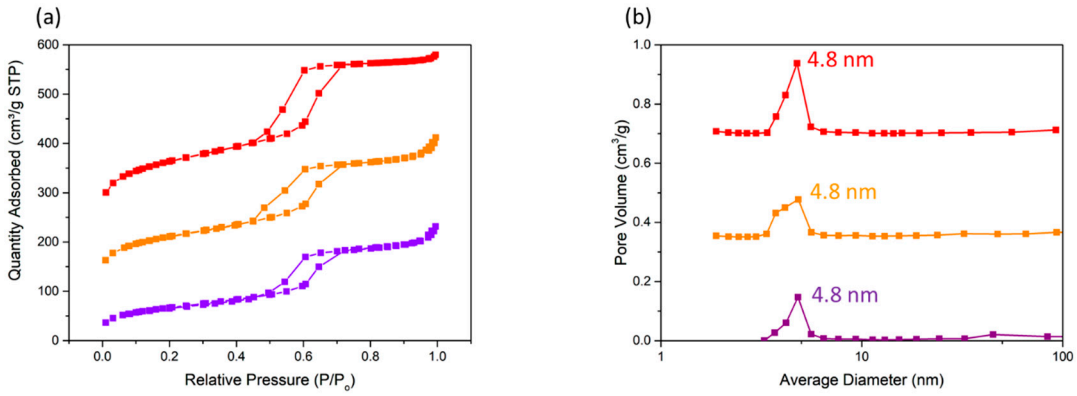

Figure 2. (**a**) Displaced BET (Brunauer–Emmett–Teller) isotherms of SBA-15 (red), IL-Cl-SBA-15 (orange), and IL-HSO_4-SBA-15 (purple) and (**b**) corresponding displaced pore size distribution profiles of SBA-15 (red), IL-Cl-SBA-15 (orange), and IL-HSO_4-SBA-15 (purple), the numbers beside the peaks indicate the diameter at the maximum.

The parent SBA-15 material, as expected, has a surface area of 552 m^2 g^{-1} and the desorption isotherm shows a H1 hysteresis loop. Functionalization of the support with the components of the HSO_4^- and Cl^--containing ionic liquids still yielded materials that gave the Type IV isotherm with H1 hysteresis loop to be maintained. However, there was a decrease in the surface areas upon functionalization. The pore volume also decreased, while the pore diameter increased. The values obtained are still in keeping with literature values [16].

There is a small broad peak in the pore size distribution profile of IL-HSO_4-SBA-15, ranging between 24–84 nm, this leads to the higher average pore size measured.

TEM images of the parent SBA-15 material and the two IL-modified analogues are shown in Figure 3. Figure 3a,b shows a typical TEM image of SBA-15 taken perpendicular to the pore channels and confirms the characteristic long-range open pore channels that are associated with its framework. This characteristic feature is typical for a mesostructure with 2D p6mm hexagonal symmetry [24,25]. Figure 3b is taken parallel to the pore channels and shows the hexagonal pores associated with SBA-15. The average channel size of SBA-15 was found to be 3.2 ± 0.6 nm (n = 30), which is in keeping with literature values [20,26], but found to be somewhat lower than values obtained by treatment of N_2 physisorption isotherm data (4.3 nm).

The discrepancies between the TEM channel (pore) sizes and BJH pore sizes is unexpected as BJH is generally thought to underestimate the pore sizes of materials [27]. It is thought that the discrepancies between the two arise from the fact that only the pore channel is measured using TEM, whereas N_2 physisorption measurements measure every pore (including macros-pores between SiO_2 particles) which contributes to a larger average pore size.

Following the tethering of ionic liquid components (Figure 3c,d), it is possible to see that the long-range order, open pore channels in (a) (IL-HSO_4) and the hexagonal pore shape in (b) (IL-Cl) remain intact.

The average channel size of the IL materials are 2.9 ± 0.5 nm (n = 50) for IL-HSO_4-SBA-15 and 3.1 ± 0.4 nm (n = 50) for IL-Cl-SBA-15. These values are somewhat lower than for the parent material, showing that tethering of the synthesized ILs does seem to decrease the channel or pore size but does not affect the overall structural integrity of the support.

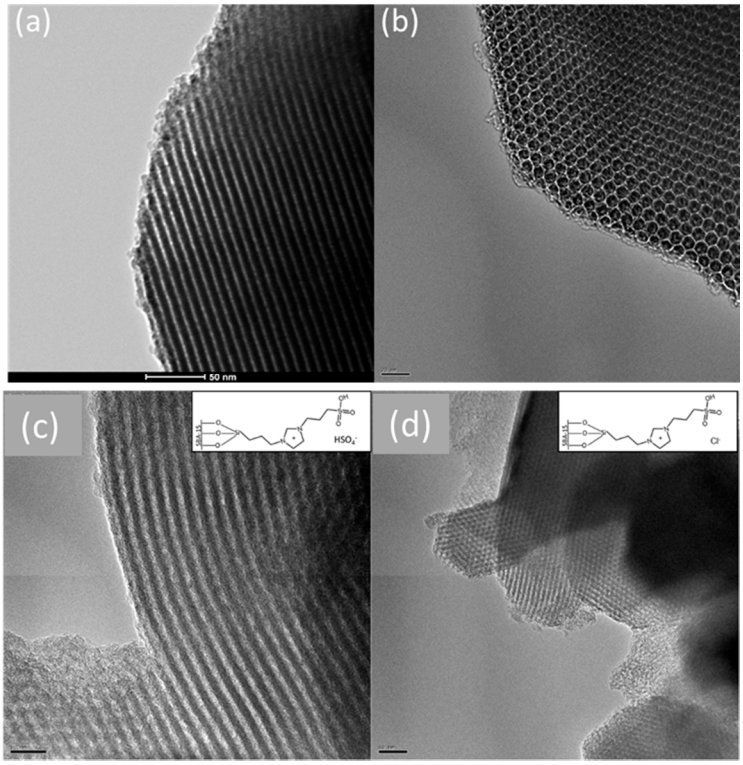

Figure 3. TEM images of SBA-15 showing (**a**) long range order open pore channels (scale bar 50 nm) and (**b**) hexagonal shaped pores (scale bar 20 nm), (**c**) IL-HSO_4-SBA-15 (scale bar 20 nm) and (**d**) IL-Cl-SBA-15 (scale bar 50 nm).

Thermogravimetry was used to confirm the tethering of the IL to the surface of the SBA. TGA of SBA-15 showed the expected profile for a pre-calcined sample, i.e., a mass loss at low temperatures (~100 °C) as adsorbed H_2O was removed from the surface and then a smaller mass loss at higher temperatures as surface hydroxyl condensation (to form removable water) took place. Mass spectrometer profiles confirmed H_2O evolution while no CO_2 was noted in the exit gas. Total mass loss following treatment to 800 °C was ~1.5%.

Figure 4 shows the TGA and DTGA profiles when the HSO_4—containing ionic liquid and the IL-HSO_4-SBA-15 catalyst were analyzed by thermogravimetry (along with the associated mass spectrometer profiles of selected exit gases).

The pure IL HSO_4 sample completely combusted in three major events (peaking at ~200, 350, and 550 °C) with concomitant evolution of CO_2, NO_2, SO_2, H_2O, and propyl fragments. No evidence of Si species in the gas phase (or remaining on the weighing pan following the experiment) was noted, and this suggests the formation and removal of an undetected gaseous species (possibly a silicon alkoxide).

Once tethered to SBA-15, the weight loss from the IL-HSO_4-SBA-15 composite material following TGA was ~26% (see Figure 4c) and again CO_2, H_2O, and SO_2 are noted in the exhaust gas. The evolution of NO_2 (which arises from the combustion of the imidazolium ring) is not noted, and it is possible that this is below the limit of detection of the mass spectrometer. The mass losses (when water desorption is ignored) confirm the expected loadings of the HSO_4 IL onto the SBA-15 material.

The relative importance of the three combustion events noted when the IL combusts prior to tethering are changed following tethering, and the material appears to be more resistant to oxidation–with the principal peak maximum moving from ~350 to ~400 °C.

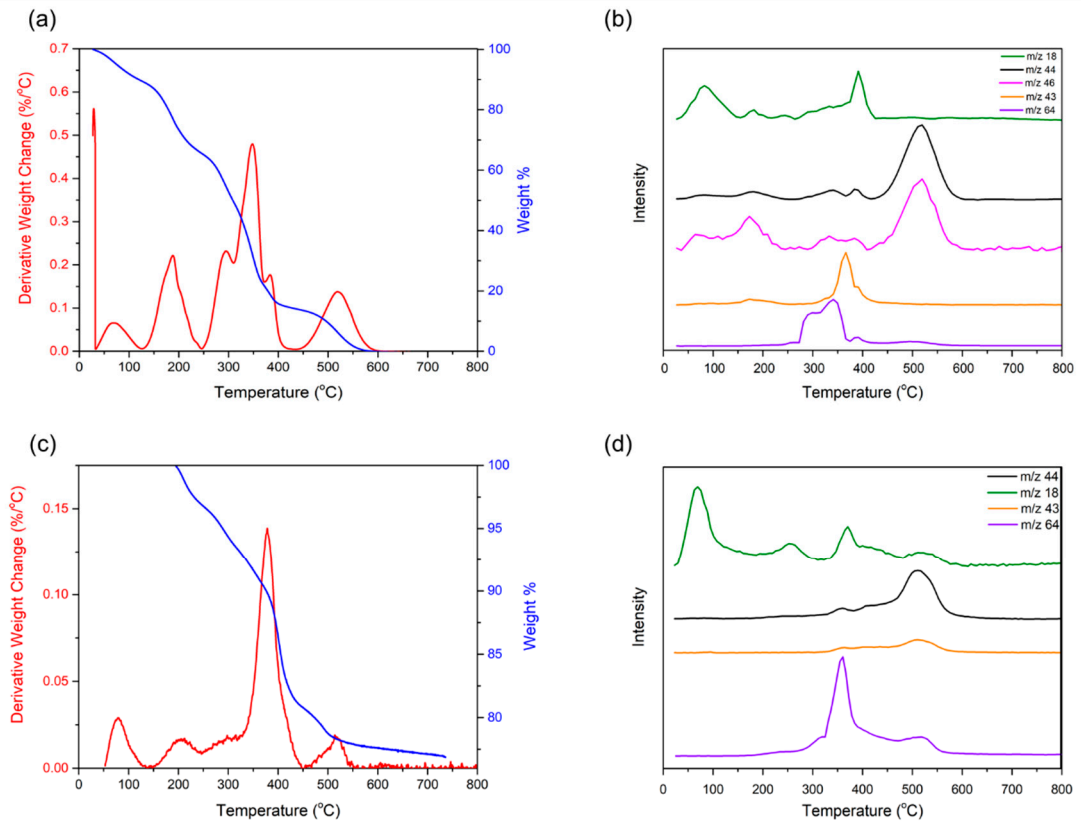

Figure 4. Differential Thermogravimetric Analysis (DTGA) and weight-loss profiles from IL-HSO_4 (**a**) and IL-HSO_4-SBA-15 (**c**), red = DTGA, blue = % weight-loss. Corresponding manually displaced mass spectrum profiles from IL-HSO_4 (**b**) and IL-HSO_4-SBA-15 (**d**), green = m/z 18 (H_2O), black = m/z 44 (CO_2), m/z 46 (NO_2) pink, orange = m/z 41 (C_3H_7 fragment), purple = m/z 64 (SO_2).

Figure 5 shows the equivalent profiles from the Cl-containing IL. In general, higher temperatures are required to oxidize this material—with DTGA peaks at 250, 400, and 600 °C. This suggests that the Cl^- counter ion has a stabilizing effect. The pure sample (when combusted to 900 °C) leaves a white residue (of ~16% of the initial IL mass) and the FTIR spectrum of the residue suggests the formation of a siliconoxychloride species [28,29].

During the temperature ramp, mass spectrometer profiles relating to CO_2, H_2O, NO_2, alkyl fragments, SO_2, and HCl are noted at temperatures co-incident with the DTGA mass loss peaks.

As was seen in the case of IL-HSO_4-SBA-15, tethering IL-Cl to SBA-15 changed the decomposition/oxidation temperatures of the components of the IL (see Figure 5c,d), with the highest decomposition temperature event now peaking at 550 °C and the lower and higher temperatures peaks reduced in size (comparing (a) to (c)).

As was also the case in the MS analysis of the IL-HSO_4-SBA-15 sample, NO_2 was not detected evolving from IL-Cl-SBA-15, again suggesting that the amounts of NO_2 generated are below the limits of detection of the mass spectrometer. A similar situation relates to attempts to monitor HCl formation during this experiment (i.e., it was visible during oxidation of the pure IL, but not during the oxidation of the tethered species).

Again, the overall mass loss (~20% in this case) is in the same range as would be expected given the amount of IL coordinated to the surface.

In conclusion, the TGA results show that both ILs are tethered to the SBA-15 surface and also show that both the tethering and the different counter-ions affect the stability of the cationic component.

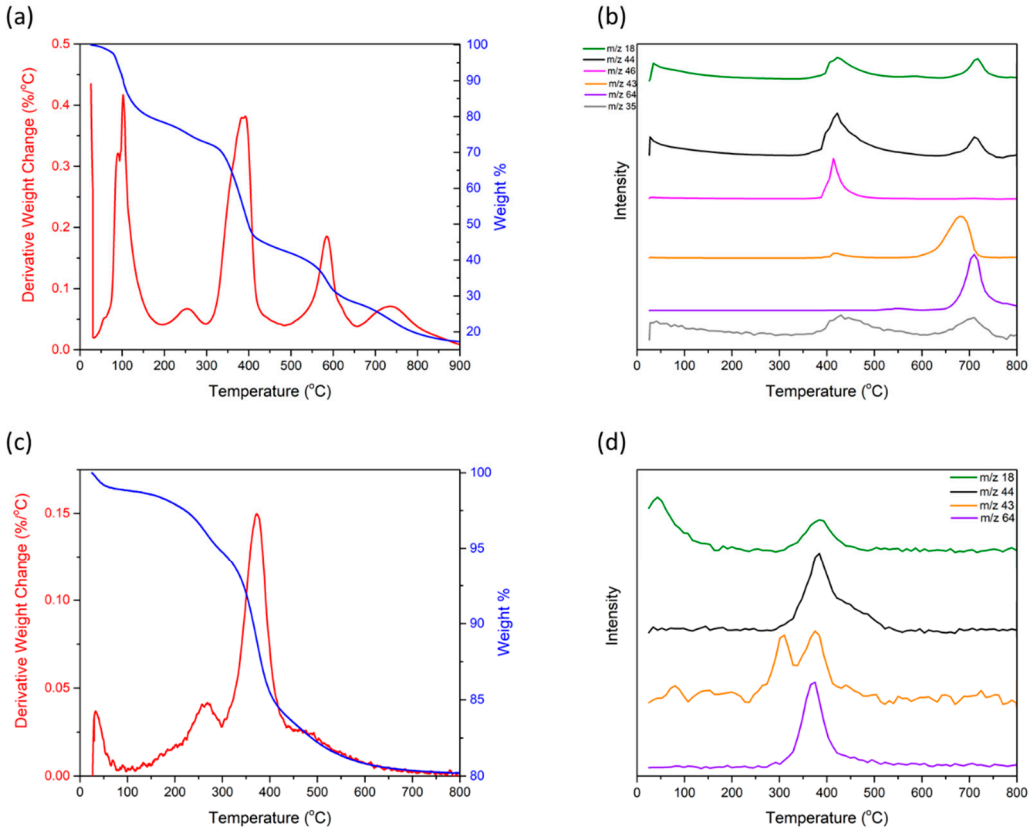

Figure 5. DTGA and weight-loss profiles from IL-Cl (**a**) and IL-Cl-SBA-15 (**c**), red = DTGA, blue = % weight-loss. Corresponding manually displaced mass spectrum profiles from IL-HSO_4 (**b**) and IL-HSO_4-SBA-15 (**d**), green = m/z 18 (H_2O), black = m/z 44 (CO_2), m/z 46 (NO_2) pink, orange = m/z 43 (C_3H_7 fragment), purple = m/z 64 (SO_2), grey = m/z 35 (Cl).

Figure 6 shows the FTIR spectrum of the two ionic liquids, Il-HSO_4 (blue) and IL-Cl (orange). The ILs cation structure is shown as an inset.

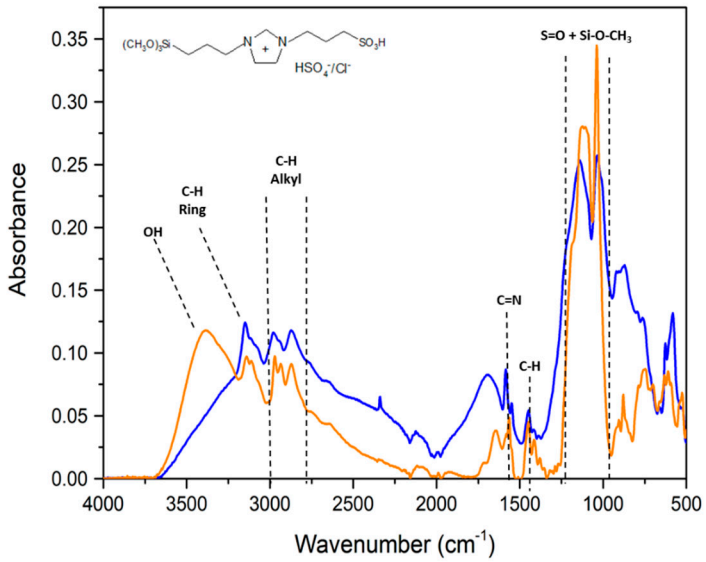

Figure 6. FTIR spectrum of acidic IL, 1-(propyl-3-sulfonate)-3-(3-trimethoxysilylpropyl) imidazolium hydrogen sulfate/chloride ([SO_3H-PIm-CPMS][HSO_4]/[Cl]), IL-HSO_4 (blue) and IL-Cl (orange).

The peaks found at 3152 and between 3000–2961 cm^{-1} are associated with C-H stretches of both the imidazolium ring and the alkyl chain, respectively. Another C-H stretch is found at 1457 cm^{-1} and is due to deformation vibrations of the alkyl chain. At 1589 cm^{-1} the stretching vibration of C = N can be observed, and this corresponds to C-N bonds within the imidazolium ring. Finally, peaks located between 1110–990 cm^{-1} are those of the Si-O-CH_3 stretching vibrations. Peaks that attributed to sulfonic acid S = O and were relevant HSO_4^- are within this region [16] and cannot be seen due to the overlap with bands relating to the Si-O-CH_3 peaks.

In addition, of note in the IL-Cl spectrum is the presence of an OH band between 3600–3300 cm^{-1}. This feature could be due to hydrogen bonding of water molecules to the IL, or possibly due to Si-OH groups formed following hydrolysis of Si-O-CH_3 [30].

Figure 7 shows the FTIR spectra of SBA-15 (red), IL-HSO_4-SBA-15 (green), and IL-Cl-SBA-15 (purple). When IL is attached to the surface of SBA-15, the peak at 3745 cm^{-1} (which relates to vibrations of isolated silanols on the SBA-15 surface) decreases in intensity. This confirms that these species are involved with the condensation reaction with the alkoxy silane groups on the IL cations.

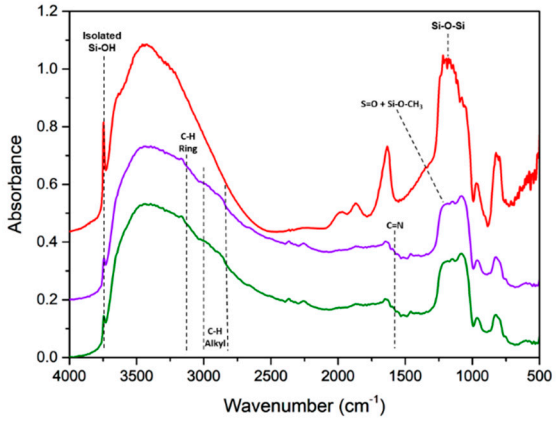

Figure 7. Displaced FTIR spectra of SBA-15 (red), IL-HSO_4-SBA-15 (green), and IL-Cl-SBA-15 (purple).

The hydrocarbon stretches of both the imidazolium ring and alkyl chains are present in both the spectra tethered IL spectra, peaking at 3152 cm^{-1} and between 3000–2961 cm^{-1}, respectively. There is also evidence for the presence of the C = N bond in the spectra of tethered ILs, with a small peak at 1589 cm^{-1}. Stretching vibration peaks of S = O and Si-O-CH_3 should be present at 1208 cm^{-1} and between 1110–990 cm^{-1} but overlap with peaks associated with the Si-O-Si, occurring between 1200–1350 cm^{-1} (the peak at 1338 cm^{-1} is noted in the SBA-15 (red) spectrum for reference).

3.2. Catalyst Acidicy Characterization

In another FTIR characterization, D-FTIR of the materials were collected following their interactions with NH_3(g). In these experiments the catalyst was used as the spectral background, and the spectra are plotted as absorbance vs. cm^{-1}. Therefore, absorbance in the spectra correspond to features added to the surface following adsorption of NH_3, and peaks pointing downwards correspond to features removed from the surface following its interaction with NH_3. Literature reports [31,32] suggest that positive peaks at 1681 and 1450 cm^{-1} can be attributed to Brønsted acids, due to the formation of the ammonium ion (NH_4^+) while positive peaks found at 1630 cm^{-1} are a result of NH_3 coordination to Lewis acid sites.

The difference FTIR spectra of NH_3 adsorbed on SBA-15 (red), IL-Cl-SBA-15 (orange), and IL-HSO_4-SBA-15 (purple) catalysts in the regions of 4000–2000 cm^{-1} (a) and 1900–1300 cm^{-1} (b) are shown in Figure 8.

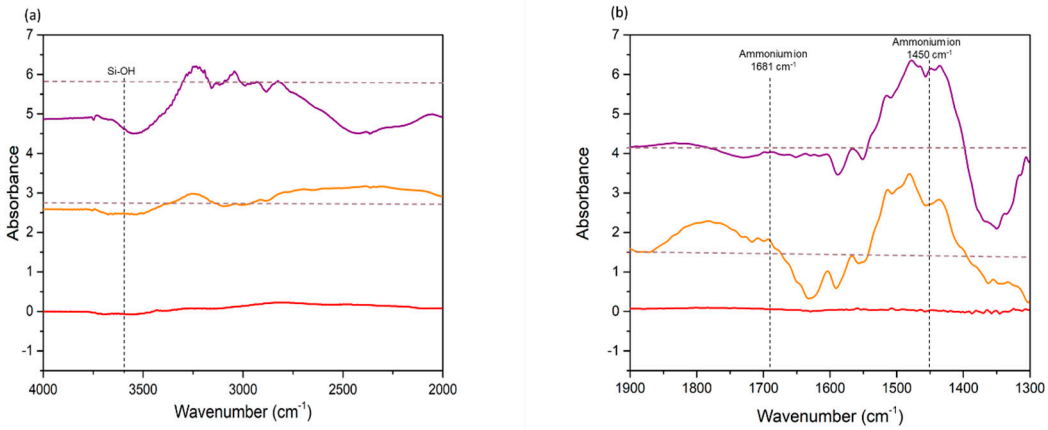

Figure 8. Displaced difference FTIR of SBA-15 (red), IL-HSO_4-SBA-15 (purple), and IL-Cl-SBA-15 (orange) after exposure to NH_3 in the regions of 4000–2000 cm^{-1} (**a**) and 1900–1300 cm^{-1} (**b**). All difference spectra used the corresponding fresh catalyst as a background.

There was no evidence for adsorption of NH_3 onto the surface of unmodified SBA-15. The spectra in (a) confirm the coordination of NH_3 with surface silanol groups (note the negative band 3600–3400 cm^{-1}) of the modified catalysts.

Both negative and positive peaks can be observed in the 1900–1300 cm^{-1} spectra (b). The negative peaks found at 1630 (on the Cl-containing catalyst) and 1589 cm^{-1} (on both catalysts) are due to the disappearance of a surface feature related to surface silanols and NH_3 adsorption to the imidazolium (C-N stretching vibration) ring, respectively (confirming adsorption on these functionalities).

Relatively intense bands are observed between 1600–1400 cm^{-1}. These relate to adsorbed NH_3 acting as a Brønsted base (i.e., forming NH_4^+). These bands have an irregular shape suggesting the overlap of several different NH_4^+ species (e.g., adsorbed on support, tether SO_3H species) making deconvolution of the positive and negative peaks in this region difficult.

Another positive peak at 1681 cm^{-1} is observed in the spectrum of NH_3 adsorbed on the IL-Cl-SBA-15 catalyst.

These experiments suggest that (a) the tethered IL are able to adsorb NH_3 and (b) there is a difference between how NH_3 interacts with IL-HSO_4-SBA-15 and how it interacts with IL-Cl-SBA-15 (note two NH_4^+ peaks on the chloride-containing sample).

The NH_3 temperature programmed desorption was also used to characterize the acidity of the catalysts. Figure 9 shows the NH_3 TPD profiles from the surface of SBA-15 (red), IL-Cl-SBA-15 (orange), and IL-HSO_4-SBA-15 (purple). These profiles have been manually displaced.

No NH_3 desorbed from the SBA-15 material. Conversely, the NH_3 profile from IL-Cl-SBA-15 evolved one broad NH_3 desorption peak, between 180–560 °C and the catalyst had an NH_3 adsorption capacity of 29 μmol NH_3 g^{-1}. Given that the desorption peak is so broad it is difficult to quantitatively describe the acid strength of the catalyst, but it is clear that a wide range of strengths are present.

The IL-HSO_4-SBA-15 profile had more well-defined desorption peaks, the first between 220–400 °C and the second (and larger) peak between 410–650 °C. It should be recalled that the tethers themselves decompose at these temperatures, and may generate NH_3 during this decomposition (although no NH_3 was noted during experiments where none had been dosed to either of these catalysts).

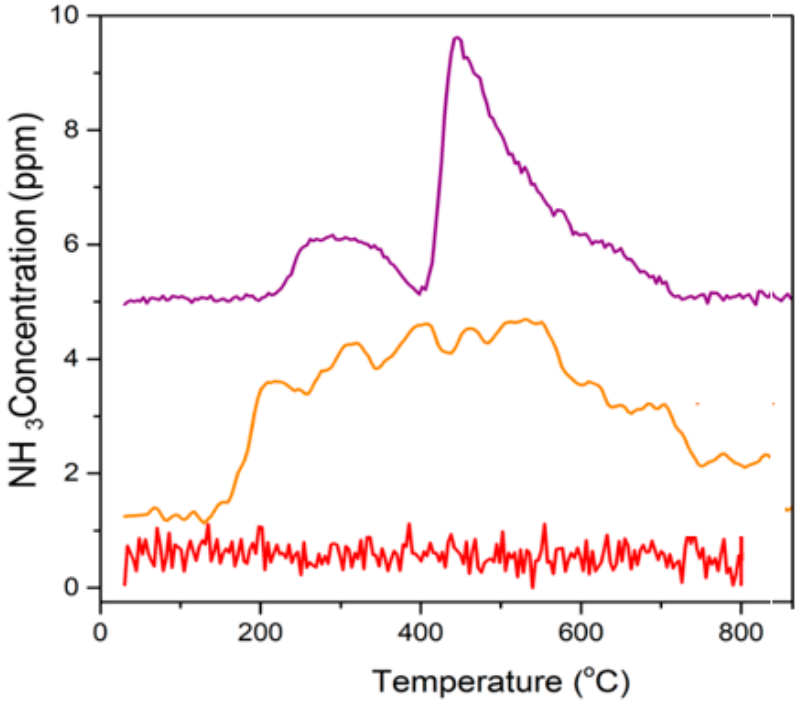

Figure 9. Displaced NH_3 Temperature Programmed Desorption (TPD) profiles from SBA-15 (red), IL-Cl-SBA-15 (orange), and IL-HSO_4-SBA-15 (purple).

This second (higher strength) adsorption site has a higher adsorption capacity than the first adsorption site (64 and 12 μmol g^{-1} NH_3 desorption, respectively). It is probable that the HSO_4^- counterion associated with this tethered ionic liquid component played a role in the NH_3 adsorption. This counterion has effectively doubled the [S] content but should also be of sufficient acid strength to coordinate NH_3. It is clear, according to this measurement that IL-HSO_4-SBA-15 has a higher concentration of acid sites than IL-Cl-SBA-15.

The S content, and therefore the number of tethered species on IL-Cl-SBA-15 and IL-HSO_4-SBA-15, are 925 and 1437 μmol g^{-1}, respectively (based on [S] measured during the elemental analysis). However, the amount of NH_3 adsorbed on (and desorbed from) each catalyst during NH_3 TPD is far lower, i.e., IL-Cl-SBA-15 and IL-HSO_4-SBA-15 desorb 29 and 76 μmol g^{-1}, respectively. This indicates that a significant proportion of tethered acid sites (more than 95% in total, be they SO_3H or HSO_4^-) are unavailable for NH_3 adsorption during the adsorption steps of these experiments.

This low adsorption capacity may be related to the interaction of tethered SO_3H groups with free surface OH groups. These may then remain 'flat-lying' on the surface hydrogen bonding to these surface OH groups (and therefore be unavailable for NH_3 adsorption).

Acid capacity measurements were used to determine the number of available H^+ g^{-1} of catalyst and can be used as a comparative measure to the NH_3 TPD results.

The catalysts were titrated with NaOH (0.01 M) using phenolphthalein (0.5 wt% in ethanol and water (1:1)) as an indicator with a color change from cloudy white to cloudy pink being associated with the neutralization point [33,34].

This shows SBA 15 as having 0.14 mmol H^+ g^{-1}, while of the two IL catalysts, IL-Cl-SBA-15 had 0.37 mmol H^+ g^{-1} and IL-HSO_4-SBA-15 had the highest concentration of available acid sites, with a concentration of 1.9 mmol g^{-1}.

Finally, regarding characterization of acidity, Hammett indicators [23] were used to give a range of acid strengths of the materials. Each indicator has a specific pKa–the lower the pKa the stronger the acid. By placing the Hammett indicators on the surface of the catalyst a pKa range for the surface acid strength can be found. If the color is that of the acid form of the indicator, then the value of the

H_0 function of the solid is equal to or lower than the pKa of the conjugate acid of the indicator. This experiment confirmed that SBA and IL-Cl-SBA-15 had pKa values between 4.8 and 0.8 (being acidic to methyl red but not to crystal violet indicators), while IL-HSO_4-SBA-15 had a pKa between 0.8 and −3.0 (being acidic to crystal violet, but not to dicinnamalacetone).

These results confirm that, notwithstanding the fact that the SO_3H loadings were comparable in both catalysts, the IL-Cl-SBA-15 acid sites were both weaker and less concentrated than those of IL-the HSO_4-SBA-15 catalyst. This must relate to an effect of the HSO_4^- counter ion, possibly acting as an acid site.

3.3. Reactivity Measurements

The reactivity of SBA-15 and both IL catalysts were probed in the VA + V-OH esterification reaction, under the experimental conditions outlined in the experimental section. The reactivity of these heterogeneous catalysts were compared to that of a model homogeneous catalyst (ρ-toluene sulfonic acid) [35] and reactions in the absence of catalyst. When catalyzed, these reactions were carried out with similar concentrations of SO_3H to allow comparisons of reactivity.

Figure 10a–d shows the removal of VA and the formation of PV in the absence of catalyst and the presence of unmodified SBA-15 (a), in the presence of a homogeneous catalyst p-toluene sulfonic acid (at the same levels as the sulfonic acid on each of the IL-SBA catalysts) (b), in the presence of IL-HSO_4-SBA-15 (c) and IL-Cl-SBA-15 (d).

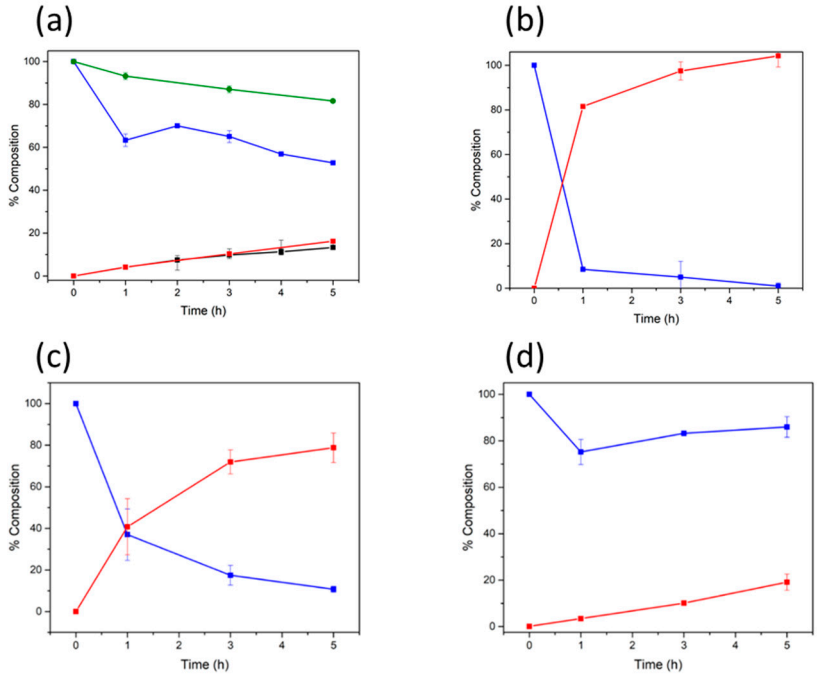

Figure 10. (**a**) Removal of valeric acid (VA) in the absence of catalyst (green) and in the presence of SBA-15 (blue) and formation of pentyl valerate (PV) in the absence of catalyst (black) and in the presence of SBA-15 (red) (**b**) reaction in the presence of p-toluene sulfonic acid, (**c**) in the presence of IL-HSO_4-SBA-15, and (**d**) in the presence of IL-Cl-SBA-15 (red is the production of PV and blue is the removal of VA in each case).

The un-catalyzed reaction forms as much PV as the reaction in the presence of unmodified SBA-15 (~13% after 5 h reaction) although the latter does remove significantly more VA (through adsorption rather than reaction). This is reflected in the carbon balance of the reaction over unmodified SBA-15 (66% after 5 h).

The reaction in the absence of added catalyst is catalyzed by the VA reactant (which itself can donate a proton to initiate the reaction).

Figure 10b shows the removal of VA and the formation of PV in the reaction in the presence of a homogeneous catalyst (p-toluene sulfonic acid) at -SO_3H loadings equivalent to those used in the tethered IL catalyzed reactions. Over 90% of the VA is converted to PV after 1 h during this reaction (showing how active sulfonic acid catalysts can be).

Figure 10c,d shows the conversions of VA and the formation of PV over both of the tethered IL materials and it is clear that, while both are significantly less active than the homogeneous analogue, the IL-HSO_4-SBA-15 catalyst (forming 78% of the possible PV product after 5 h) is far more active than the IL-Cl-SBA-15 material (forming 19% of the possible PV product after 5 h).

The tethered IL catalysts also show far higher carbon balances than the unmodified SBA-15 (90% and 99% compared to 66%). This suggests that surface hydroxyls are the adsorption sites for VA on SBA-15 and their removal (through condensation in the preparation of the tethered IL catalysts) hinders this adsorption.

The reactivity of the IL-Cl-SBA-15 and IL-HSO_4-SBA15 catalysts were measured in a recyclability experiment. In these reactions the used catalysts were washed in CH_3OH and dried at 80 °C overnight before reuse.

The reactivity over both catalysts was lower than the activity of the analogous fresh catalyst. In the case of the IL-Cl-SBA-15 material, conversion to PV fell to the same level as was seen in the uncatalyzed reaction (or the reaction over SBA-15), while in the case of the IL-HSO_4-SBA-15 catalyst, conversion after 5 h conversion to PV fell from 78% to 60%.

The IL-HSO_4-SBA-15 catalyst had a higher acidity (both in terms of concentration and acid strength) than IL-Cl-SBA-15 and also had a higher activity in promotion of the desired reaction. The extent of the difference between the reactivity of the two materials is somewhat surprising considering that both catalysts have the same cation and (to a first approximation) the same surface concentration of HSO_3.

It is clear that the different counterions have an effect on both the acidity and the activity of the catalyst (and it is assumed that the former influences the latter).

The IL-Cl-SBA-15 catalyst appears to have no significant catalytic effect whereas the catalyst containing the HSO_4^- counter ion appears to have a substantial beneficial effect on the activity of the catalyst.

It is possible that the HSO_4^- ion itself is also acting as a catalyst. This species can potentially donate a proton (initiating the reaction). However, HSO_4^- is considered a weak acid with a pKa of +1.9 and a K_a of 1.2×10^{-2}, whereas H_2SO_4, for example, with a pKa of 3.0 and a K_a of 1×10^3 [36]. Given that it is such a weak acid it may simply be coordinating the reactants to the surface of the catalyst, orienting them for reaction as opposed to donating a proton and initiating the reaction.

Post-reaction characterization was also carried out on the three materials.

TGA profiles from post reaction SBA-15 show a mass loss of 17.5% (compared to 1.5% mass loss from the fresh catalyst). The fresh catalyst lost mass during TGA from dehydration and dihydroxylation, while the post reaction catalyst lost mass due to combustion of adsorbed VA from the reaction mixture (D-FTIR analysis of post reaction SBA-15 confirms a carbonyl stretch of adsorbed VA and not PV).

FTIR of the post-reaction IL-HSO_4-SBA-15 and IL-Cl-SBA-15 catalysts also shows evidence for VA (and not PV), adsorption on both materials and this relates to the measured carbon balances (which were 90% and 99% over the IL-HSO_4-SBA-15 and IL-Cl-SBA-15 catalysts, respectively).

TGA from the post reaction IL-HSO_4-SBA-15 and IL-Cl-SBA-15 catalysts (results not shown) show that, notwithstanding the adsorption of some reactants on the catalysts, the mass losses from the post-reaction materials during TGA were lower than those from the fresh IL-HSO_4-SBA-15 and IL-Cl-SBA-15 catalysts.

The fresh IL-HSO_4-SBA-15 catalyst lost 19.7% during TGA while the post-reaction catalyst lost 17.6% of its mass. The fresh IL-Cl-SBA-15 lost 18.8% of its mass during TGA, while its post reaction analogue lost 14.9% of its mass.

These results suggest that some of the tethered species were removed (possibly hydrolyzed with water produced during the esterification reaction) from the surface during the reactions.

4. Conclusions

Two catalysts containing a tethered IL cation ((1-(propyl-3-sulfonate)-3-(3-propyl) imidazolium) with Cl^- and HSO_4^- counter ions were prepared and characterized. Both catalysts contained approximately equivalent loadings of the IL components. The acid strength and concentrations on the Cl^- catalyst were significantly lower than those of the HSO_4^- material. While both materials were less active than a homogeneous analogue in promoting the esterification reaction, the HSO_4^--containing catalyst was far more active than the Cl^--containing material. It is thought that the S-containing counter-ion either acts itself as an acidic catalyst in the reaction (possibly in solution) or plays a role in orienting reactants for reaction. The tethered cation was not stable under reaction conditions with TGA confirming loss of portions of the tether from the surface following reaction.

Author Contributions: The research was conceived and directed, and the manuscript produced by J.A.S. L.M. performed the experiments and wrote preliminary drafts. All authors have read and agreed to the published version of the manuscript.

Funding: This research received no external funding.

Acknowledgments: The UCD School of Chemistry is acknowledged and thanked for providing a studentship for L.M.

Conflicts of Interest: The authors declare no conflict of interest.

References

1. IPCC. *Climate Change 2013: The Physical Science Basis. Contribution of Working Group I to the Fifth Assessment Report of the Intergovernmental Panel on Climate Change*; Stocker, T.F., Qin, D., Plattner, G.-K., Tignor, M.M.B., Allen, S.K., Boschung, J., Nauels, A., Xia, Y., Bex, V., Midgley, P.M., Eds.; Cambridge University Press: Cambridge, UK; New York, NY, USA, 2013; p. 1535.
2. Flach, B.; Lieberz, S.; Rossetti, A. EU Annual Biofuels. 2017. Available online: https://apps.fas.usda.gov/newgainapi/api/report/downloadreportbyfilename?filename=Biofuels%20Annual_The%20Hague_EU-28_6-19-2017.pdf (accessed on 21 June 2017).
3. Sherry, L.; Sullivan, J.A. The reactivity of mesoposrous silica modified with acidic sites in the production of Biodiesel. *Catal. Today* **2011**, *175*, 471–476. [CrossRef]
4. Sherry, L.; Sullivan, J.A. Different dispersions of group II catalysts over SBA-15 and MCM041: Effects on transesterification reactivity. *Catal. Commun.* **2015**, *60*, 88–91. [CrossRef]
5. Tomei, J.; Helliwell, R. Food versus fuel? *Going beyond biofuels Land Use Policy* **2016**, *56*, 320–326. [CrossRef]
6. Yi, Z.; Hu, D.; Xu, H.; Wu, Z.T.; Zhang, M.; Yan, K. Metal regulating the highly selective synthesis of gamma-valerolactone and valeric biofuels from biomass-derived levulinic acid. *Fuel* **2020**, *259*, 116208. [CrossRef]
7. Rackemann, D.W.; Doherty, W.O.S. Biofuels Bioprod. *Biorefin* **2011**, *5*, 198–214. [CrossRef]
8. Lange, P.; Price, R.; Ayoub, P.M.; Louis, J.; Petrus, L.; Clarke, L.; Gosselink, H. Valeric Biofuels: A Platform of Cellulosic Transportation Fuels. *Angew. Chem. Int. Ed.* **2010**, *49*, 4479–4483. [CrossRef]
9. Mullins, L.; Sullivan, J.A. Synthesis of a Sustainable Cellulose-Derived Biofuel through a 1-Pot, 2-Catalyst Tandem Reaction. *Top. Catal.* **2020**, 1–12. [CrossRef]
10. Jeenpadiphat, S.; Bjork, E.M.; Oden, M.; Tungasmita, D.N. Propylsulfonic acid functionalized mesoporous silica catalysts for esterification of fatty acids. *J. Phys. Chem. C* **2015**, *410*, 253–259. [CrossRef]
11. de Assis, J.V.; Abranches, P.A.S.; Braga, I.B.; Zuniga, O.M.P.; Sathicq, A.G.; Romanelli, G.P.; Sato, A.G.; Fernandes, S.A. p-Sulfonic acid calix[4]arene-functionalized alkyl-bridged organosilica in esterification reactions. *RSC Adv.* **2016**, *6*, 24285–24289. [CrossRef]

12. Liu, C.-Z.; Wang, F.; Stiles, A.R.; Guo, C. Ionic liquids for biofuel production: Opportunities and challenges. *Appl. Energy* **2012**, *92*, 406–414. [CrossRef]
13. Parvulescu, V.; Hardacre, C. Catalysis in Ionic Liquids. *Chem. Rev.* **2007**, *109*, 2615–2665. [CrossRef] [PubMed]
14. Zhen, B.; Li, H.; Jiao, Q.; Li, Y.; Wu, Q.; Zhang, Y. $SiW_{12}O_{40}$-Based Ionic Liquid Catalysts: Catalytic Esterification of Oleic Acid for Biodiesel Production. *Ind. Eng. Chem. Res.* **2012**, *51*, 10374–10380. [CrossRef]
15. Liu, Y.; Wang, Y.; Zhai, C.; Chen, W.; Qiao, C. Kinetics study of the esterification reaction of diethylene glycol monobutyl ether with acetic acid catalyzed by heteropolyanion- based ionic liquids. *Ind. Eng. Chem. Res.* **2014**, *52*, 14633–14640. [CrossRef]
16. Zhang, L.; Cui, Y.; Zhang, C.; Wang, L.; Wan, H.; Guan, G. Brønsted Acidic Ionic Liquid Modified Magnetic Nanoparticle: An Efficient and Green Catalyst for Biodiesel Production. *Ind. Eng. Chem. Res.* **2012**, *51*, 16590–16596. [CrossRef]
17. Zhang, P.P.; Kang, L.H.; Tong, Y.B.; Deng, C.M.; Zhu, M.Y.; Dai, B. An ionic liquid supported on zirconia-modified silica as a catalyst for oxidative desulfurization. *J. Pet. Sci. Eng.* **2020**, *193*, 107386. [CrossRef]
18. Qian, C.W.; Yao, C.S.; Yang, L.J.; Yang, B.; Liu, S.C.; Liu, Z.T. Preparation and Application of Silica Films Supported Imidazolium-Based Ionic Liquid as Efficient and Recyclable Catalysts for Benzoin Condensations. *Catal. Lett.* **2020**, *150*, 1389–1396. [CrossRef]
19. Kaur, P.; Chopra, H.K. Recent Advances in Applications of Supported Ionic Liquids. *Curr. Org. Chem.* **2019**, *23*, 2881–2915. [CrossRef]
20. Zhao, D.; Sun, J.; Li, Q.; Stucky, G.D.; Barbara, S. Morphological Control of Highly Ordered Mesoporous Silica SBA-15. *Chem. Mater.* **2000**, *12*, 275–279. [CrossRef]
21. Rahmat, N.; Abdullah, A.Z.; Mohamed, A.R. A review: Mesoporous Santa Barbara amorphous-15, types, synthesis and its applications towards biorefinery production. *Am. J. Appl. Sci.* **2010**, *7*, 1579–1586. [CrossRef]
22. Mueller, R.; Kammler, H.K.; Wegner, K.; Pratsinis, S.E. OH Surface Density of SiO_2 and TiO_2 by Thermogravimetric Analysis. *Langmuir* **2003**, *19*, 160–165. [CrossRef]
23. Yurdakoç, M.; Akçay, M.; Tonbul, Y.; Yurdakoç, K. Acidity of silica-alumina catalysts by amine titration using Hammett indicators and FT-IR study of pyridine adsorption. *Turkish J. Chem.* **1999**, *23*, 319–327.
24. Thielemann, J.P.; Girgsdies, F.; Schlog, R.; Hess, C. Pore structure and surface area of silica SBA-15: Influence of washing and scale-up. *Beilstein J. Nanotechnol.* **2011**, *19*, 110–118. [CrossRef]
25. Zhao, D.; Feng, J.; Huo, Q.; Melosh, N.; Fredrickson, G.H.; Chmelka, B.F.; Stucky, G.D. Triblock Copolymer Syntheses of Mesoporous Silica with Periodic 50 to 300 Angstrom Pores. *Science* **1998**, *279*, 548–552. [CrossRef] [PubMed]
26. Kokunesoski, M.; Gulicovski, J.; Matovic, B.; Logar, M.; Milonjic, S.K.; Babic, B. Synthesis and surface characterization of ordered mesoporous silica SBA-15. *Mater. Chem. Phys. J.* **2010**, *124*, 1248–1252. [CrossRef]
27. Rocha, J.V.; Barrera, D.; Sapag, K. Improvement in the pore size distribution for ordered mesoporous materials with cylindrical and spherical pores using the Kelvin equation. *Top. Catal.* **2011**, *54*, 121–134. [CrossRef]
28. Launer, P.J.; Arkles, B. *Infrared Analysis of Organosilicon Compounds: Spectra-Structure Correlations*; Gelest Inc.: Morrisville, PA, USA, 2013; p. 19067.
29. Ullal, S.J.; Singh, H.; Vahedi, V.; Aydil, E.S.; Ullal, S.J. Deposition of silicon oxychloride films on chamber walls during Cl_2 / O_2 plasma etching of Si. *J. Vac. Sci. Technol.* **2012**, *499*. [CrossRef]
30. Mohan, J. *Organic Spectroscopy: Principles and Applications*, 2nd ed.; Alpha Science International: Oxford, UK, 2002.
31. Barzetti, T.; Selli, E.; Moscotti, D.; Forni, L. Pyridine and ammonia as probes for FTIR analysis of solid acid catalysts. *J. Chem. Soc. Faraday Trans.* **1996**, *92*, 1401–1407. [CrossRef]
32. Martins, G.V.A.; Berlier, G.; Bisio, C.; Coluccia, S.; Pastore, H.O.; Marchese, L. Quantification of Brønsted acid sites in microporous catalysts by a combined FTIR and NH_3-TPD study. *J. Phys. Chem. C* **2008**, *112*, 7193–7200. [CrossRef]
33. Yang, L.M.; Wang, Y.J.; Luo, G.S.; Dai, Y.Y. Functionalization of SBA-15 mesoporous silica with thiol or sulfonic acid groups under the crystallization conditions. *Microporous Mesoporous Mater.* **2005**, *84*, 275–282. [CrossRef]
34. Testa, M.L.; La Parola, V.; Venezia, A.M. Transesterification of short chain esters using sulfonic acid-functionalized hybrid silicas: Effect of silica morphology. *Catal. Today* **2014**, *223*, 15–121. [CrossRef]

35. Lotero, E.; Liu, Y.; Lopez, D.E.; Suwannakarn, K.; Bruce, D.A.; Goodwin, J.G. Synthesis of biodiesel via acid catalysis. *Ind. Eng. Chem. Res.* **2005**, *44*, 5353–5363. [CrossRef]
36. Murdachaew, G.; Gaigeot, M.P.; Halonen, L.; Gerber, R.B. First and second deprotonation of H_2SO_4 on wet hydroxylated (0001) α-quartz. *Phys. Chem. Chem. Phys.* **2014**, *16*, 22287–22298. [CrossRef] [PubMed]